



Radiation Environment and Cosmics from Gaia at L2

prepared by: Asier Abreu
affiliation : ESAC
approved by:
reference: GAIA-CA-TN-ESAC-AAA-035-1
issue: 1
revision: 1
date: 2017-09-01
status: Issued

Abstract

The radiation environment experienced by Gaia since launch is analyzed. Cosmic ray detection rates and relation to major solar events are investigated in an attempt to understand better the radiation environment at L2 during solar events.

Document History

Issue	Revision	Date	Author	Comment
0	1	2015-08-01	AAA	First Draft
1	0	2015-10-01	AAA	Consolidated Version
1	1	2015-10-26	AAA	Final additions and Issued
1	2	2015-10-31	AAA	External comments and new references included. Revision of section 3.3 performed in view of the comments received.
1	3	2017-09-01	AAA	Modified document number due to clash at Livelink repo with CalteamUplink 15.0 SRN

Contents

1 Motivation	4
2 Cosmic rays in the object detection process	5
3 PPE counters	6
3.1 Overview	6
3.2 Long Term PPE counters behavior and Solar Activity	8
3.3 Rotational modulation on the PPE counters	11
3.3.1 Stray-light study case:	12
3.3.2 'FPA to Sun' orientation study case	17
3.3.3 Conclusion	19
4 Solar Particle Events	20
4.1 Major Solar Events	20
4.2 Solar Particle Event Energy Distribution at L2 ?	25
5 Conclusions	27
6 References	28

1 Motivation

The nominal lifetime of Gaia mission , assuming no major spacecraft anomalies , will be determined to a good extent by the nominal lifetime of it's detectors. Radiation damage accumulated through time affects the charge transfer efficiency (CTE) of the Gaia CCD devices causing a progressive degradation of their performance and ultimately determining the nominal regime in which science data can still be collected usefully.

Serial and Parallel Charge Transfer efficiencies are regularly monitored and measured onboard Gaia through specific calibration activities and the analysis of the FPR (First Pixel Response) from virtual objects with Charge Injection. These give an estimation of the radiation damage accumulated up to the time of execution of the activity.

However Gaia only has limited 'direct' measurements of the instantaneous radiation environment at L3 and certainly no measurement of the cosmic ray energy distribution. Preliminary work on energy and time distribution of the cosmics was presented by Floor Van Leeuwen in FVL-144 for one solar event.

This note tries to provide further insight on this and other aspects of the L2 radiation environment through investigation of a broader set of solar events occurred so far and the comparison with data taken from other satellites.

Note on Time Scales:

Throughout this note the Gaia DPAC time scale is used, OBMT in units of revolutions (1 rev=6 hrs). When using data from other spacecrafts however, UTC time scale is used as the 'common' time scale. Conversion between Obmt and UTC is provided by the Obmt decoder DPAC tool available at : <http://gaia.esac.esa.int/gaiafe/decoder/obmtDecoder.jsp>.

External Data Sources:

Several external data sources have been used in this technical note:

- Solar activity historical data: Source: WDC-SILSO, Royal Observatory of Belgium, Brussels: <http://www.sidc.be/silso/datafiles>
- ESA's Space Radiation Environment Monitor (SREM) : Source : ESA Space Environment web portal: http://space-env.esa.int/index.php/SREM_Plots.html
- NASA's Advance Composition Explorer data (ACE) and GOES data : Source : (SOHO FTP: <ftp://sohoftp.nascom.nasa.gov/sdb/>

2 Cosmic rays in the object detection process

Gaia VPUs are in charge of objection detection onboard. This detection process takes place in the SkyMappers (SMs) were the flux coming from each image area sample set from FoV1 and FoV2 SM CCDs are verified for local maxima. The VPU detection algorithms then 'discriminate' non-star like objects from stars by means of their PSF shape (See GAIAASF.UM.PLM.00022 Sec. 13). Amongst those non-star like objects are of course cosmic rays which are regularly hitting the Gaia CCDs at L2. Statistics about this detection process , how many rejected cosmics (Prompt Particle Events counts), how many rejected star ripples (Rejected Ripple counts), how many stars, are collected by the VPUs and downlinked in the form of auxiliary science ASD4 telemetry packets.

For illustration a full frame engineering (not standard) image of the Sky Mapper 1 where a number of cosmic ray trails can be visible.



Figure 1: Prompt Particle Event hits detected visible in the in SM1 CCD readout full frame.

This information can therefore be used to determine the instantaneous cosmic ray hit rates as seeing by Gaia in L2. We will now look in more detail in particular to these Prompt Particle Event (PPE) statistics which account for cosmics.

3 PPE counters

3.1 Overview

The following is an example of the Prompt Particle Event rates (PPE counts) as extracted from the ASD4 auxiliary science data for VPU1 in both FOVs:

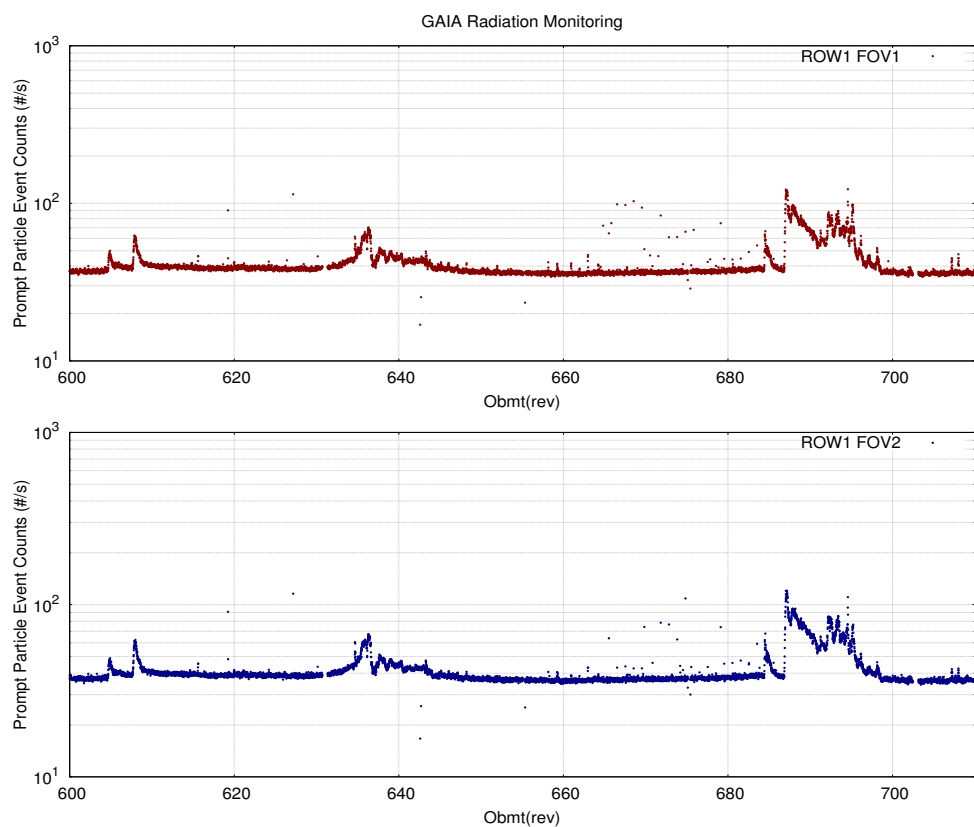


Figure 2: Prompt Particle Event Rates as detected by VPU1 in SM1 (red) and in SM2 (blue) during April 2014.

These counters represent the only *direct* radiation environment measurement that Gaia performs. Nevertheless the plots already show how increased radiation activity can be tracked directly at least in statistical terms. Several bursts of solar activity can be clearly seen in the plots around Obmt rev 690 (19th April 2014) and 640 (6th April 2014).

One important aspect worth noting in these PPE counters besides the actual solar activity itself, is the continuous baseline or 'pedestal' present at all times which is already appreciable in the plots from Fig. 2. This 'background' cosmic rate was originally reported (and it's origin explained) by the First Look Scientists at ARI and since then has become part of the knowledge base of the First Look Scientist Team.

Using the formalism originally presented by Jos de Bruine in GAIA.JDB.TN.026.2005 , we can estimate the 'Prompt Particle Event' rate measured at each CCD (SM or AF) produced by an incident isotropic flux of cosmics given by $F(\text{particles cm}^{-2} \text{ s}^{-1})$ as :

$$R_{\text{CCD}} = \frac{F_{\text{CCD}} \cdot A}{2} \text{counts} \cdot \text{s}^{-1} \quad (1)$$

were A is the area of the given detector in cm^2 . For SM CCDs where detection takes place the effective¹ CCD area is 17.1 cm^2 , and therefore the predicted particle hit rate assuming a typical particle flux at L2 of $5 \text{ particles cm}^{-2} \text{ s}^{-1}$ extracted from GPDB will be:

$$R_{\text{CCD}}(\text{predicted}) = \frac{5 \cdot 17.1}{2} \simeq 43 \text{counts} \cdot \text{s}^{-1} \quad (2)$$

This prediction is in good agreement with the actual background level that can be inferred from the PPE data (See Fig. 2) of ~ 40 particles s^{-1} . In fact the PPE counters baseline has evolved from an initial value of ~ 10000 counts during early 2014 to ~ 11000 counts in early 2015. Using the equation above and taking into account that ASD4 detection statistics are accumulated over $257.635\text{s} (= T_{\text{ASD4}}$ packet generation period), this results in a computed particle hit rate per second of:

$$R_{\text{CCD}}(\text{early 2014}) = \frac{10000}{257.635} \simeq 38,82 \text{counts} \cdot \text{s}^{-1} \quad (3)$$

$$R_{\text{CCD}}(\text{early 2015}) = \frac{11000}{257.635} \simeq 42,70 \text{counts} \cdot \text{s}^{-1} \quad (4)$$

These numbers show how the cosmic ray flux measured at L2 is in fact not static but evolves through the mission time.In the following section we will try to find an explanation for these evolutions in the radiation background and some practical implication of it.

¹SM CCDs are operated with Gate12 permanently on to avoid saturation from bright stars in the detection process. Taking into account Gate12 position in the CCD at 2900 TDI lines from origin, the effective detecting area in the SM CCDs is approximately 1966 columns x 2900 TDI lines x 10um x AC 30um = 17.1 cm^2

3.2 Long Term PPE counters behavior and Solar Activity

As reported in previous section the PPE counters baseline or pedestal has evolved since Gaia launch in Dec 2013 towards 2015. The following figure shows the yearly 2014 evolution of the PPE count rates for VPUs 1,4 and 7 in FOV1 (FOV2 shows equivalent trend). We also show the solar activity in that period traced by sun spot numbers:

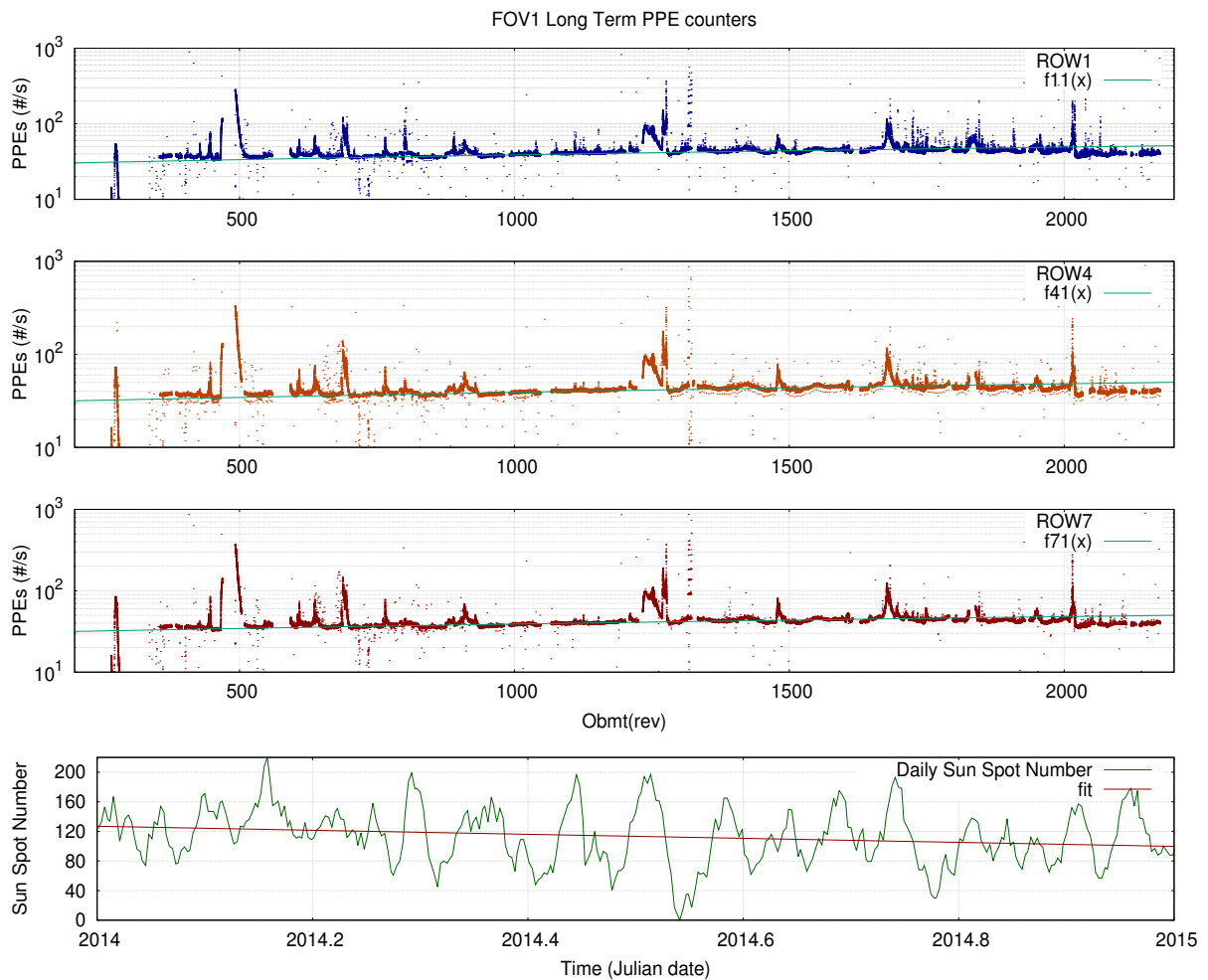


Figure 3: Long Term PPE Rate evolution. Since Gaia Launch Dec 2013 up to May 2015 for VPUs 1,4 and 7. Number of Solar Spots as a tracer for solar activity for equivalent period (bottom)

There is a clear anti-correlation between solar activity and Prompt Particle Event count rates evolution detected by Gaia in L2. This effect, anti-correlation between cosmic ray levels and solar activity is well known (Davis et al. (2001); Heber et al. (2009); O'Neill et al. (2015)) and was also detected by Herschel mission at L2 (Horeau et al. (2011)).

When exploring available radiation measurement data from past missions at L2 like Herschel , we also see there is a time evolution of the radiation environment in L2. Plots showing the Herschel SREM instrument count rates for a selected energy range at the beginning and end of the mission, period 2009-2013:

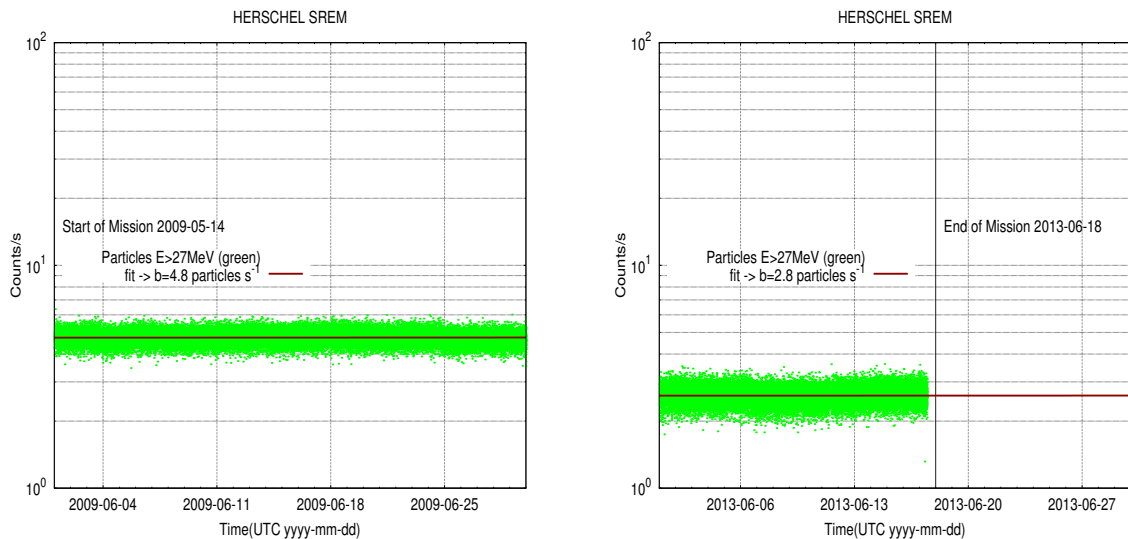


Figure 4: Herschel SREM data. Particle counts (and fit to baseline) at mission start (left) and at mission end (right) in 2013. Overall decrease in the rates measured (Energy range of $E > 27\text{MeV}$) from $4.8 \text{ particles s}^{-1}$ at mission start to $2.8 \text{ particles s}^{-1}$ at mission end.

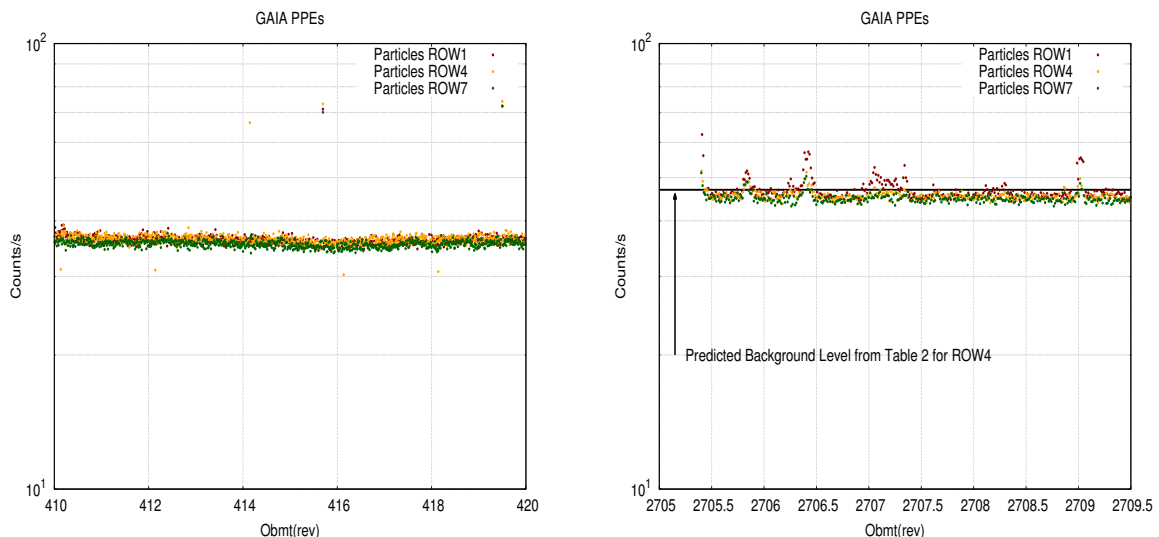


Figure 5: Gaia PPEs data. Particle counts at early mission (left) and at current mission time. Evolution of the particle flux at L2 is seen as an overall increase in the rates measured which varies from $\sim 37 \text{ particles s}^{-1}$ to $\sim 43 \text{ particles s}^{-1}$.

Table 2: Expected Galactic Cosmic Ray hit rates at time t per VPU and FOV are given by the general expression $PPE_n[FOV] = a_n[FOV] + b_n[FOV]$. Slope and intercept fit values.

VPU _n	FOV _n	Slope / Intercept
VPU1	1	0.0040 / 36.1800
VPU2	1	0.0036 / 36.9268
VPU3	1	0.0036 / 36.4399
VPU4	1	0.0040 / 36.1478
VPU5	1	0.0038 / 36.0726
VPU6	1	0.0038 / 36.0640
VPU7	1	0.0039 / 35.6964
VPU1	2	0.0039 / 36.1800
VPU2	2	0.0039 / 36.0611
VPU3	2	0.0035 / 36.4423
VPU4	2	0.0040 / 36.5040
VPU5	2	0.0027 / 38.3554
VPU6	2	0.0040 / 36.4748
VPU7	2	0.0039 / 36.4469

This cosmic ray flux-solar activity anti-correlation is mainly due to the solar magnetic field which during solar maxima provides more 'shielding' against *Galactic* Cosmic Rays for the inner Solar System. This results in a *decreasing* measured GCR background rate towards solar maximum (Fig. 4) and a *increasing* GCR background rate towards solar minimum (Fig. 5).

This in turn also indicates that the pedestal present in the Gaia PPE counters is primarily caused by Galactic Cosmic Rays on top of which increased solar activity will produce bursts of solar protons. We made simple fits to the baselines of the PPE profiles for each VPU and FOV to obtain a first order expected time evolution of the baselines. The resulting fit coefficients are provided in Table 2

These expressions can be used to extrapolate Galactic Cosmic Ray expected fluxes measured at L2 by Gaia at future points in the mission time. In the right Fig. 5 we show the predicted background level using the fits above and we can see that prediction is typically overestimating only by a few percent. **However** solar activity is not completely predictable and therefore these expressions will likely only hold as first order approximations.

3.3 Rotational modulation on the PPE counters

The long term analysis of the PPE counters has also revealed another interesting feature, modulation of these with the spin phase of the satellite. This modulation is present almost all along the mission *including* solar quiet periods and shows varying amplitude from VPU to VPU. Several examples of it:

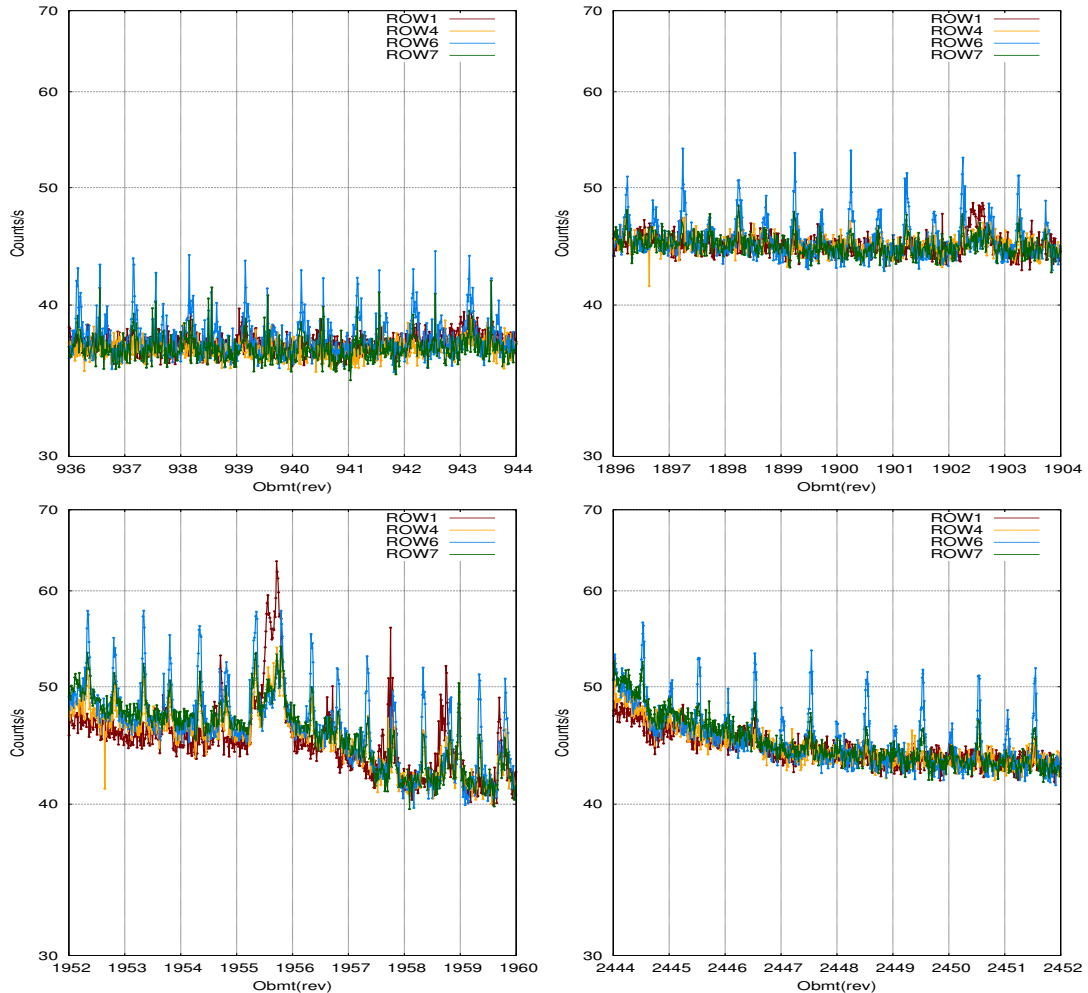


Figure 6: Rotational modulation of the PPE counters.VPUs 1,4, 6 and 7 displayed.

Due to their intrinsically periodic nature we have studied two possible causes of the features, namely:

1. **Stray-light:** stray-light from the Sun or the Galaxy entering the optical path through FOV1 or FOV2 apertures will increase background noise and could trigger false cosmic ray detections.
2. **FPA-to-Sun orientation:** spacecraft rotation could modulate the PPE signals through differential shielding in different collision paths.

3.3.1 Stray-light study case:

We selected different periods and searched for differences in the behavior of the peak features between FOV1 and FOV2 as the later is known to show stronger stray-light levels (See AB-049) .

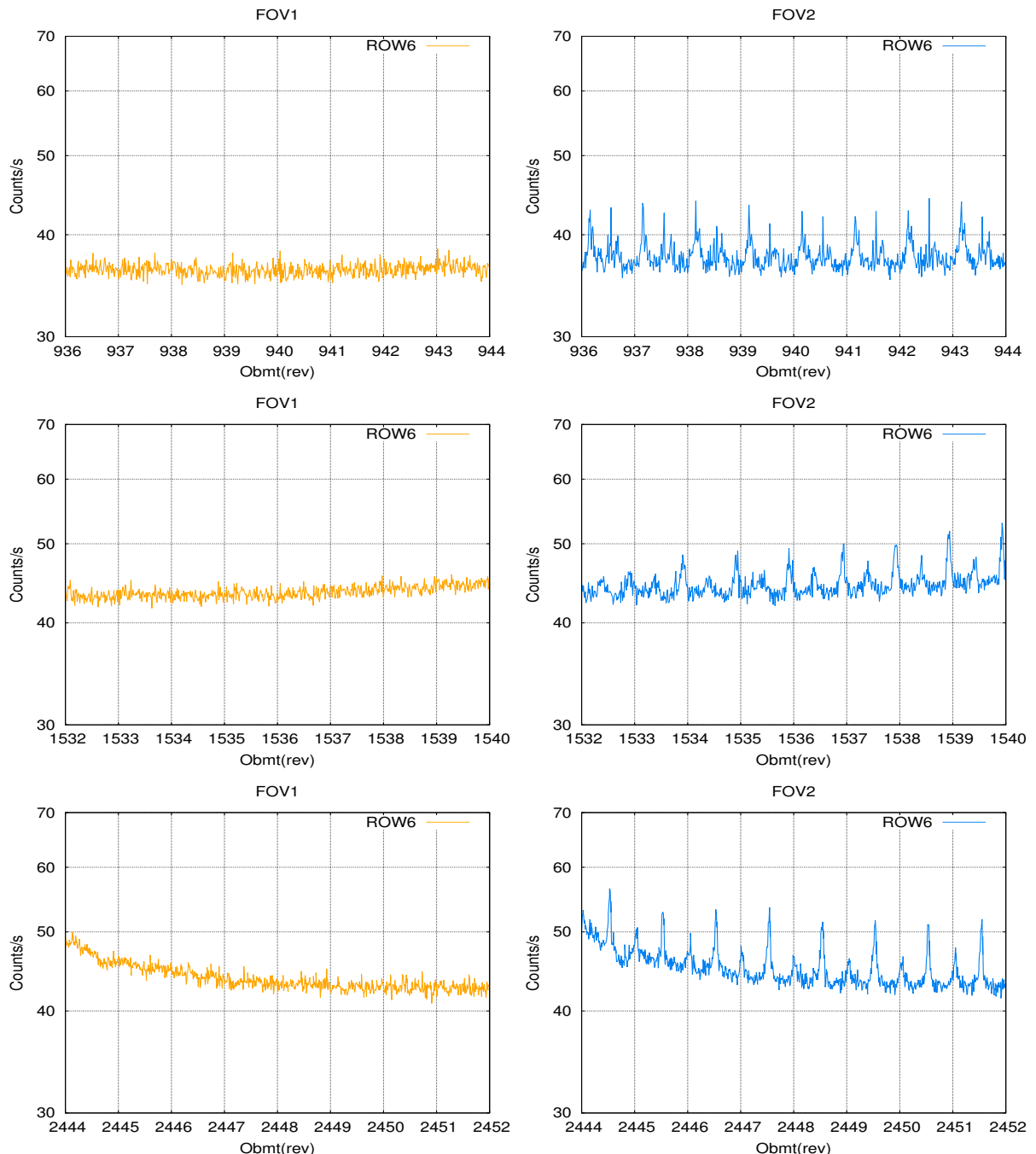


Figure 7: FOV1(left) vs FOV2(right) relative behavior of periodic features for VPU 6.

The plots in Fig. 7 show periodic peak features that are only present on FOV2 (We present only 1 VPU for the sake of plot clarity but the same behavior with lesser amplitude is present in all other VPUs). The fact that these appear only in one FOV and not the other points already to a stray-light origin, there is no reason why particles (not photons) would selectively and systematically choose to impact in one set of SM CCDs and not the other. The period of those peaks is in fact 3 hrs and is therefore tracing in this case stray-light from the Milky-Way, as Gaia will cross twice the galactic plane every 6 hrs.

We now look further into other periods. In this case we inspected a period where the 6-hr features seem to be more complex, with interleaved peak features 6-hr apart, different from the previous cases studied above. We inspected the background profile as extracted from 2D virtual object windows from FOV2 virtual objects during this period :

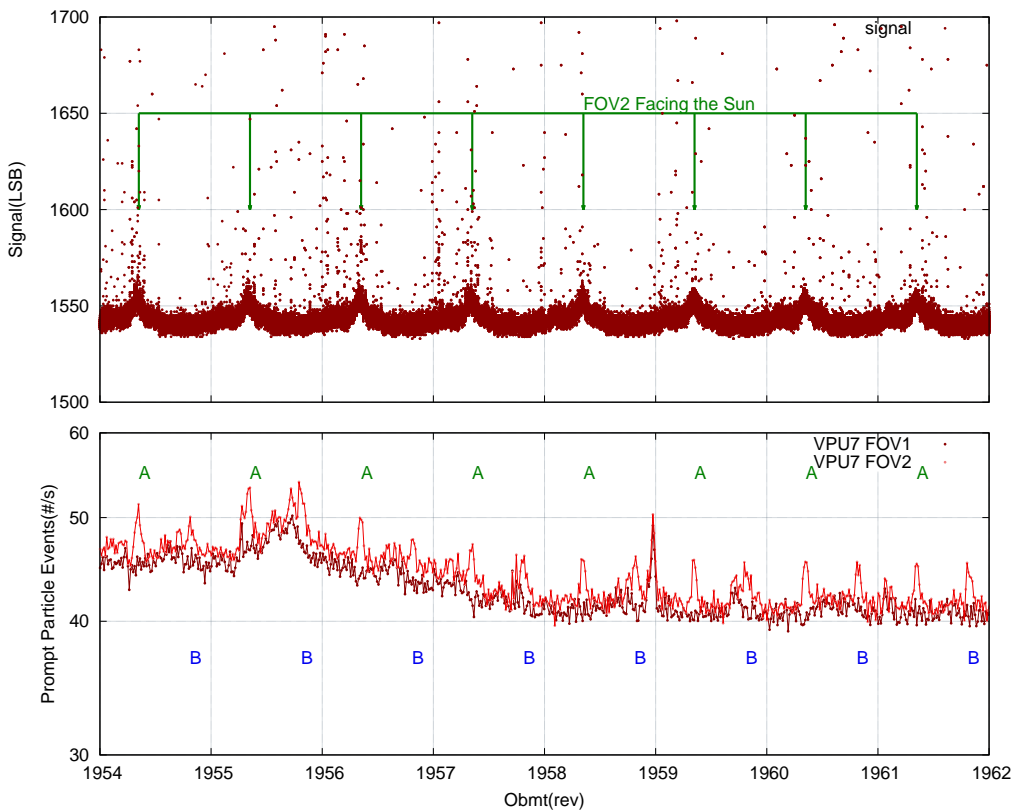


Figure 8: VPU7 background signal extracted from 2D VO windows (top). PPEs for VPU7 FOV1 and FOV2 (bottom). Stray-light favoring orientations in FOV2 are marked by green arrows and A.

There is clear match from VPU7 FOV2 PPE 6hr features with FOV2 positions 'facing the Sun'². This indicates that at least the 6 hr VPU7 FOV2 feature visible in the PPEs is caused by increased background from the Sun triggering false detections, i.e, not real cosmic rays.

² These 'stray-light favoring' orientations are those in which the centre of each FOV is pointing in the same direction as the Sun-To-Spacecraft vector, therefore increasing the amount of stray-light diffracted by the DSA reaching the top of the Thermal Tent Structure where the telescope apertures are located.

Positions where FOV2 is facing the Milky Way also show a good correlation with the features on VPU1 (top plot in the figure below). This indicates that those features in VPU1 are caused by stray-light in this case coming from the Milky-Way. A check on FOV1 facing the Milky Way shows the missing correlation for the points marked 'b' in the figure above.

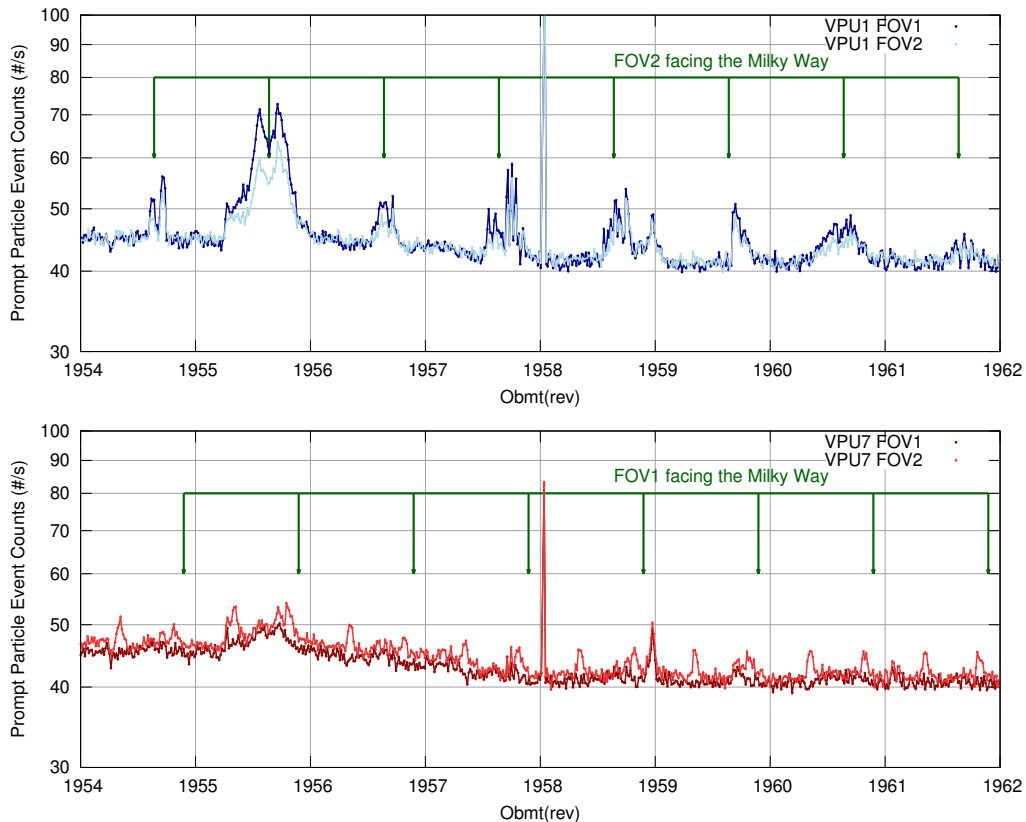


Figure 9: PPEs on VPU1(dark-blue FOVP / light-blue FOVF). In light-blue the moments at which FOV2 is facing the Milky-Way.

We have also verified that no increased solar activity was taken place during the above mentioned periods.

Further plots showing evidence of an increase in PPE detections on VPU7 FOV2 correlated with positions of the FOV2 aperture 'facing the Sun'.

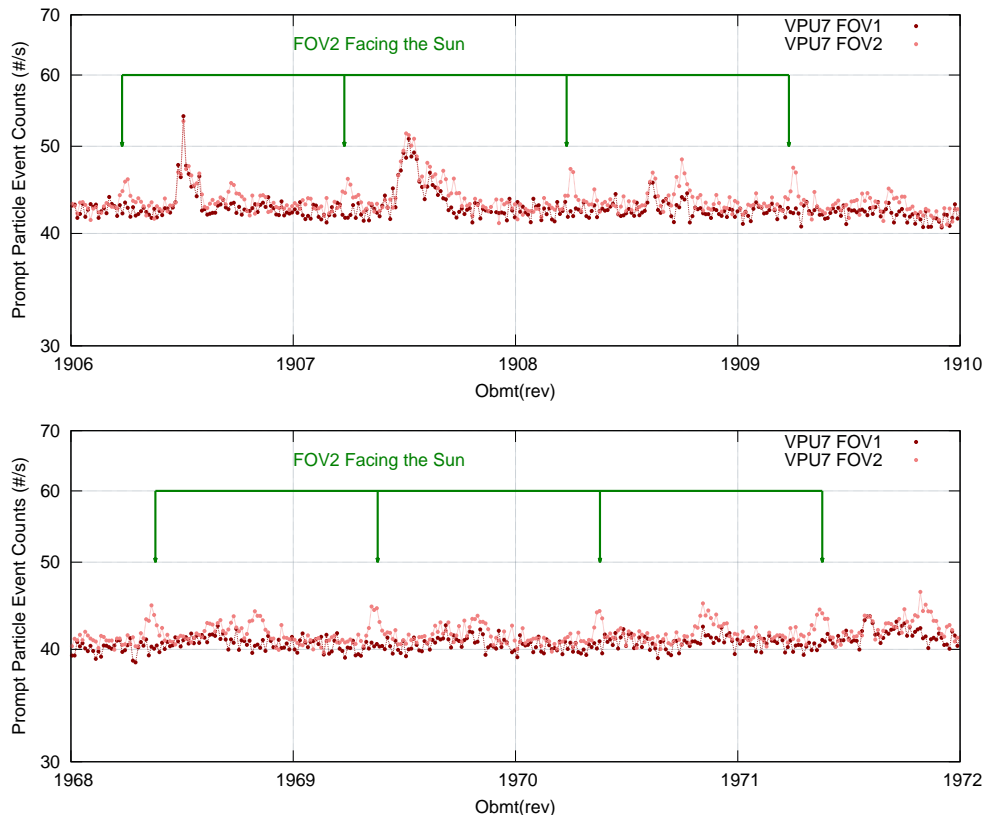


Figure 10: PPEs on VPU7(dark-red FOVP / light-red FOVF). In green the moments at which FOV2 is 'facing the Sun'.

Another favoring correlation with stray-light from the Sun can be seen in those periods where scan angle with respect to the ecliptic decreases. In these occasions an overall increase in the background level can be seen in the 'baseline' of the PPE rates and also in the VPU7 FOV2 periodic features. See figure in following page.

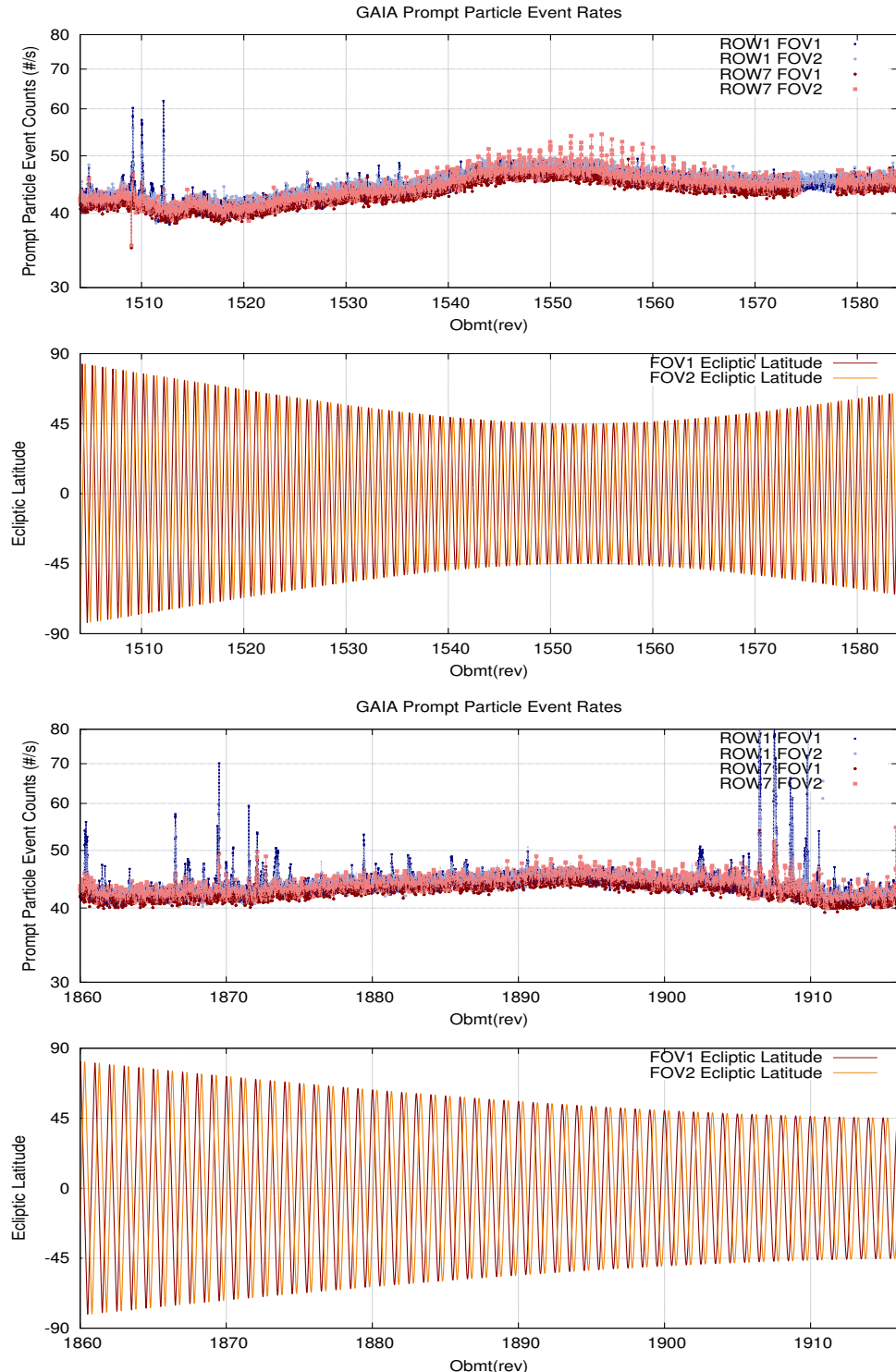


Figure 11: PPE counts (top) and ecliptic latitude (bottom) for two different periods. An overall increase in the background causing an increase in the PPEs baseline is appreciable.

3.3.2 'FPA to Sun' orientation study case

The FPA orientation with respect to the Sun can be traced using the spin phase of the satellite. If rotational modulation due to shielding is to be present it should be particularly noted during Solar Particle Events due to the inherently directional nature of the proton beam from the Sun against the omni-directional flux of galactic cosmic rays. See the next figure for a visual representation of the spacecraft Scanning Reference System and the relative position of the telescope apertures and FPA.

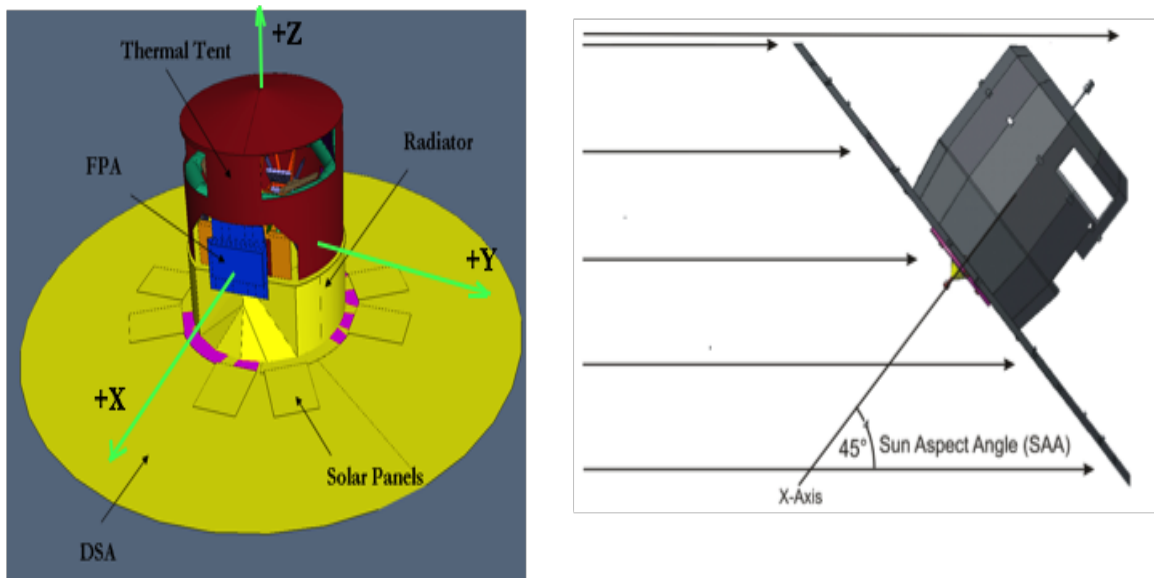


Figure 12: Gaia spacecraft and Scanning Reference System in green (LEFT): Telescope apertures FOV1 and FOV2 and FPA back part (radiator) in blue. Spin direction is anti-clock wise as seen from the Z axis. (RIGHT) :The angle between the S/C to Sun vector and the -Z axis is the Sun Aspect Angle, set to 45° for Gaia Nominal Scanning Law. The spin phase is the angle defined by the projection of the S/C to Sun vector in the Gaia scanning plane and the Gaia +X axis in the Scanning Reference System. This angle is zero when the projection of spacecraft-to-sun vector is aligned with the +X_{SRS} axis. The direction -X_{FPA} is the same direction as +X_{SRS} axis, Therefore at phase 0° the FPA is facing in the opposite direction from the Sun and shielded behind the FPA cold radiator. At phase 180° the FPA will be 'facing' the Sun. Full details on Gaia Reference Systems are provided in BAS-003

We have selected a number of 'minor' solar events in which this modulation with spin phase can be appreciated in the form of 'dips' in the PPE counters. These 'dips' are not present in the radiation profiles measured by other spacecrafts , therefore pointing to an intrinsic modulation caused by Gaia as it rotates :

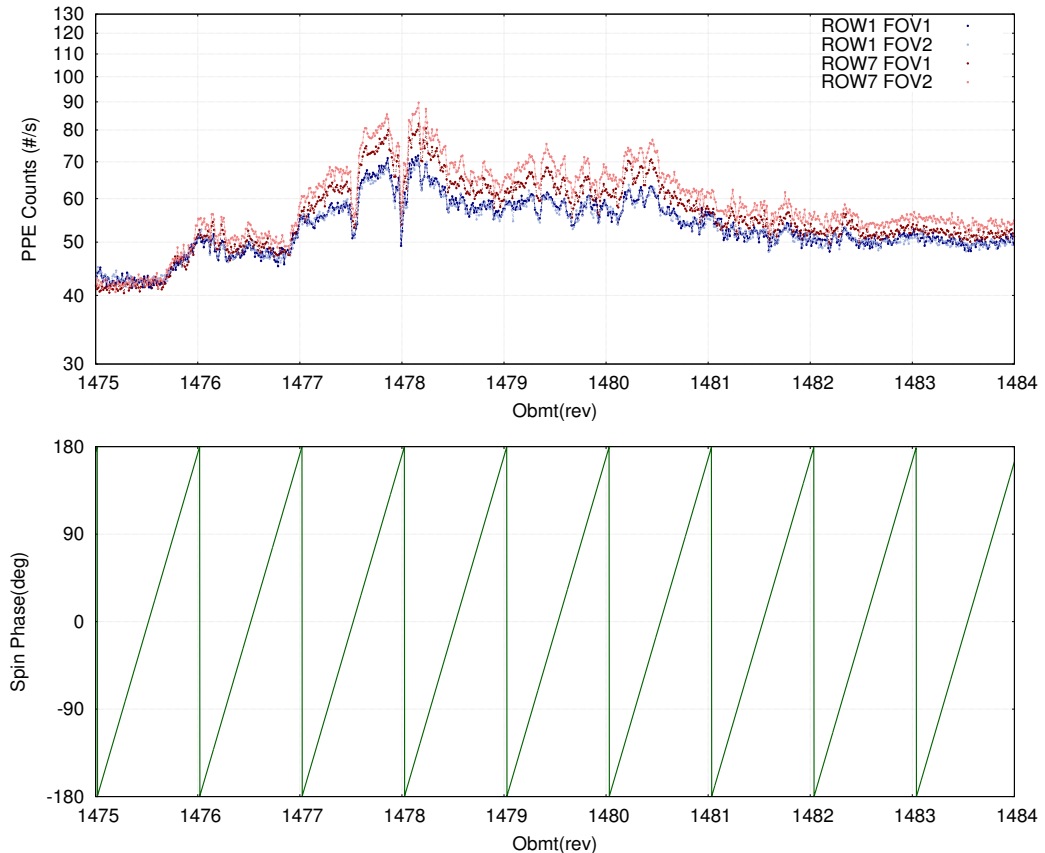


Figure 13: Gaia PPEs (top) and spin phase (bottom). December 2014. Note the 'dips' on the PPEs profile at Obmt 1477.5 and Obmt 1478).

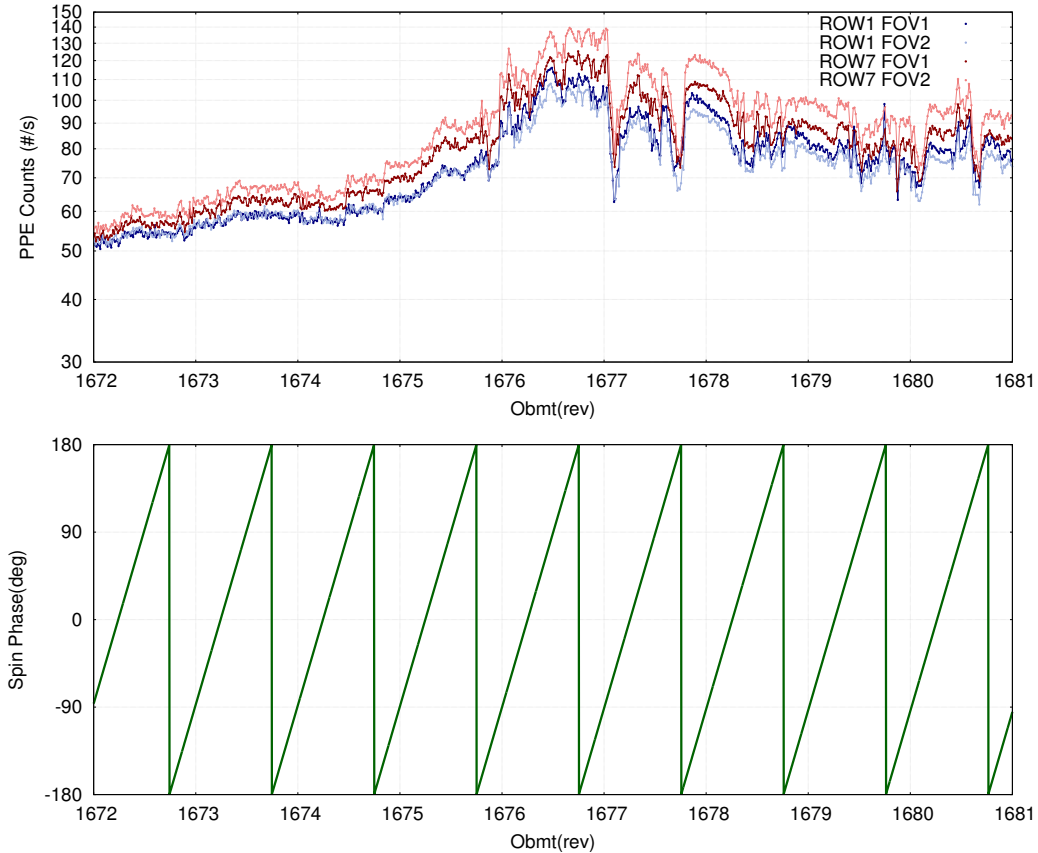


Figure 14: Gaia PPEs (top) and spin phase (bottom). November 2014. Note the 'dips' on the PPEs profile at Obmt 1677.3 and Obmt 1677.8.

These plots show some degree of rotational modulation with spin phase, but there is not enough cases of these weak events to solidly establish a relation between particular spin phases and PPE modulation. Naturally the more shielded position of the FPA with respect to incoming proton beam is that of 0° , when the FPA is shielded behind the FPA radiator and facing away from the Sun and Fig. 13 shows this potential correlation but then is not so clear in Fig. 14. The rest of solar events don't show these 'dips' in the PPE counters.

3.3.3 Conclusion

Of the possible causes studied in relation with the periodic features seen in the PPEs we conclude that a good fraction (if not all) of the 'peaks' are explained by stray-light from either the Sun or the Milky Way entering through the telescope apertures and resulting in increased background at the SM CCDs triggering false cosmic ray detections.

A larger sample of 'weak' events would need to be collected to establish solidly a correlation between particular spin phases and shielding , the 'dips' noticed occasionally the PPE counters.

4 Solar Particle Events

As stated in Section 1, although the Gaia PPE counters provide a good 'statistical' estimate of the status of the radiation environment at L2 , they are limited as no energy distribution information can be extracted from them. Moreover, there are no other spacecrafts at L2 during the duration of the Gaia mission, so 'direct' measurements of the radiation environment energy distribution at L2 during Gaia mission time are not available.

We have thus compared the Gaia radiation measurements (PPEs) to other spacecraft located near Earth and in L1 libration point, which do measure directly the radiation environment at those locations, in an attempt to find similarities in the data that could lead to a better understanding of the radiation environment at L2 during solar particle events. We will use data from the following instruments: ACE SIS (Zwickl et al. (1998)),INTEGRAL SREM (Paul Buhler (1998)) and GOES EPAM (Rodriguez et al. (2010)).

4.1 Major Solar Events

The following plots show comparisons between the particle count rates as measured by Gaia and 3 other spacecrafts , namely , INTEGRAL, GOES-15 and ACE satellites, for a number of solar events experienced so far since launch.

We have considered the following solar events³:

1. 7th January 2014 , a X1.2-class Solar Flare and CME
2. 27th February 2014 , a classified X4.9-class Solar Flare and CME
3. 12th September 2014 , a classified X1.6-class Solar Flare and CME
4. 21st June 2015, a classified M3.0-class Solar Flare and CME

³We recall here that the solar flares classification series A (weakest), B, C, M and X (strongest) is a logarithmic scale. Flare origin times have been extracted from : <http://umtof.umd.edu/pm/FIGS.HTML>. We have considered CME (Halo) which have a component directed towards Earth.

Solar Flare : January 2014

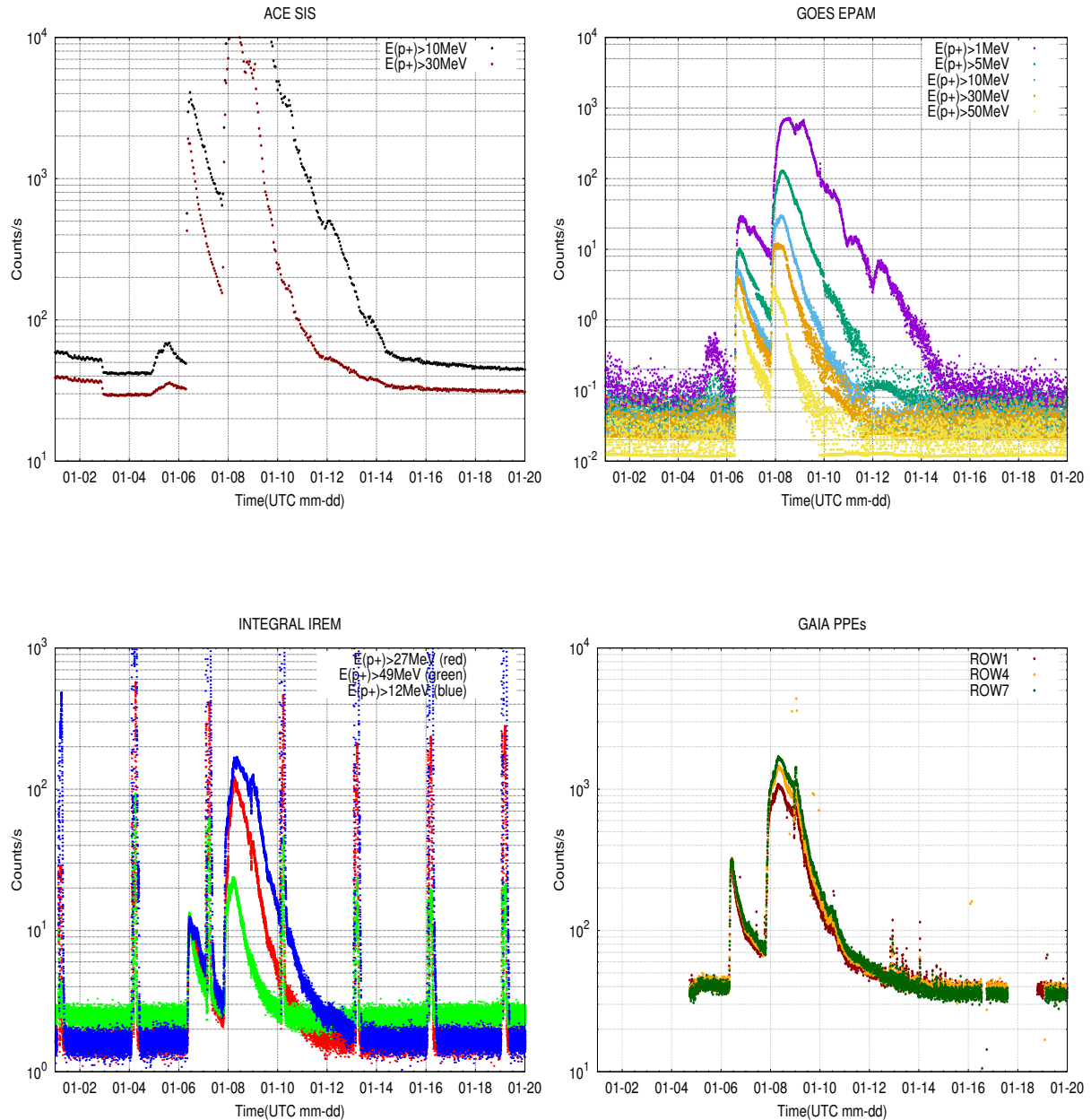


Figure 15: Particle Count Rates from ACE SIS (top left), GOES EPAM (top right), INTEGRAL SREM (bottom left : vertical features are radiation belt crossings) and GAIA PPEs (bottom right) for January 2014 Solar Event.

Solar Flare : February 2014

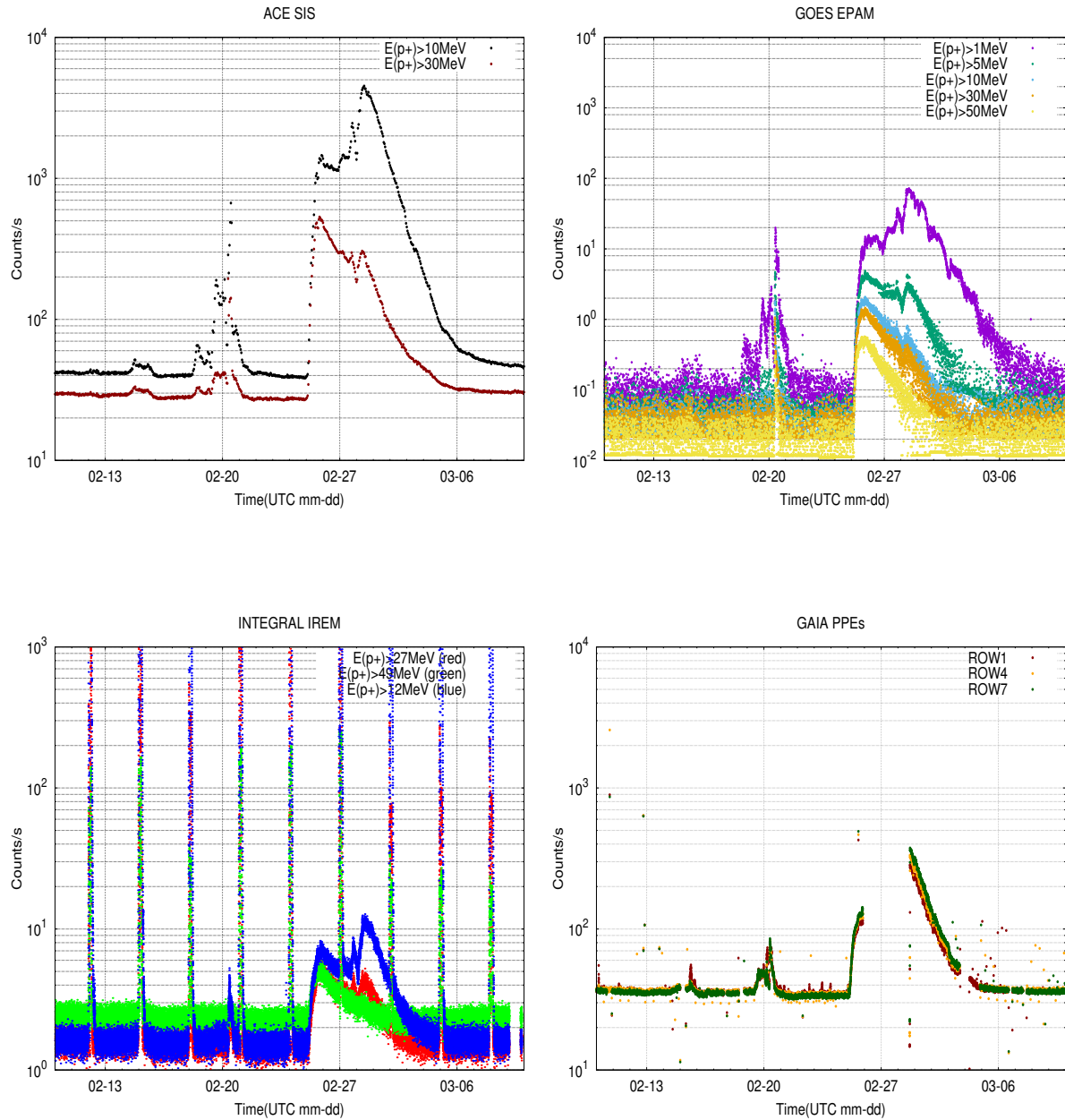


Figure 16: Particle Count Rates from ACE SIS (top left), GOES EPAM (top right), INTEGRAL IREM (bottom left : vertical features are radiation belt crossings) and GAIA PPEs (bottom right) for February 2014 Solar Event.

Solar Flare : September 2014

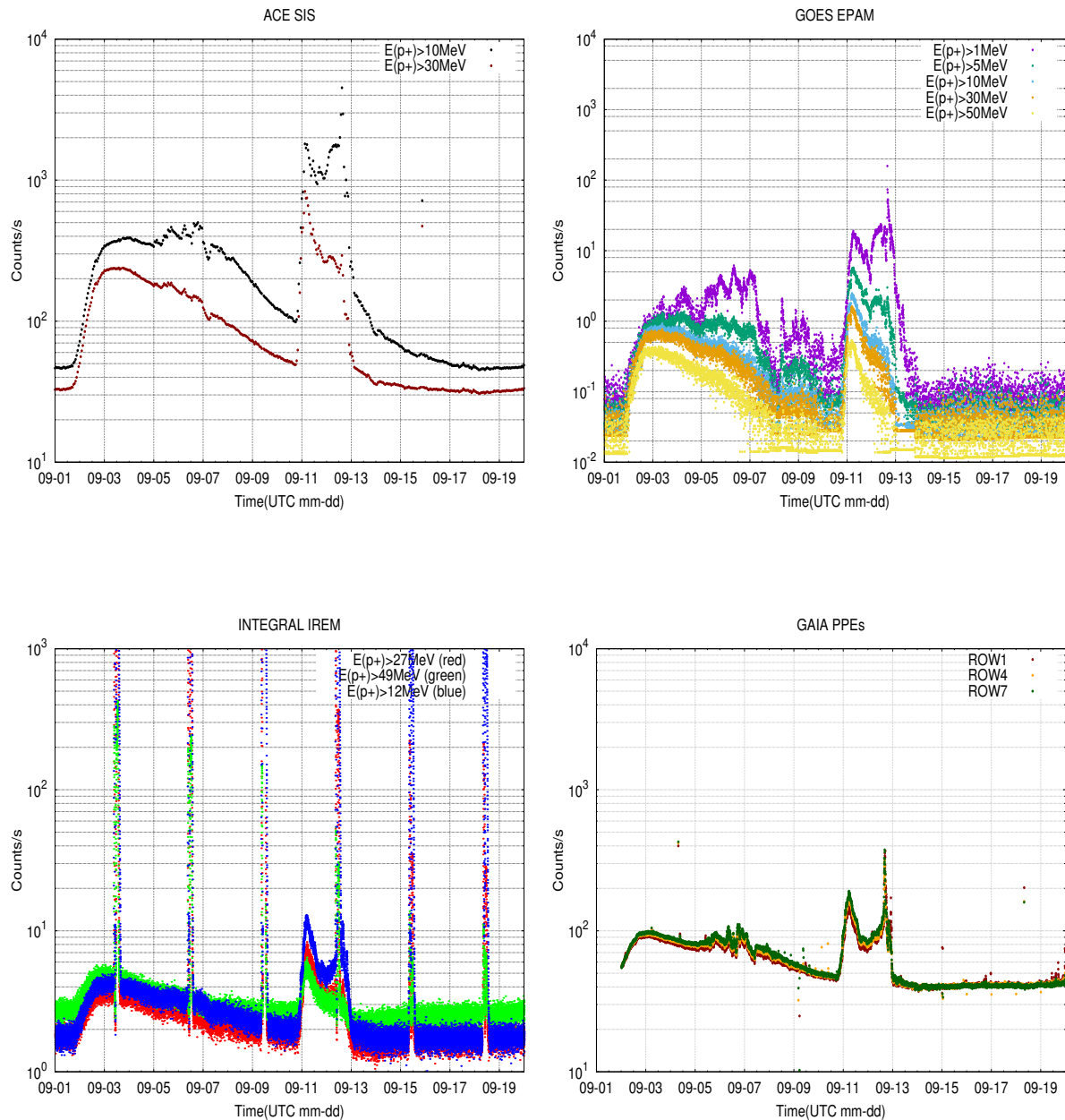


Figure 17: Particle Count Rates from ACE SIS (top left), GOES EPAM (top right), INTEGRAL IREM (bottom left : vertical features are radiation belt crossings) and GAIA PPEs (bottom right) for September 2014 Solar Event.

Solar Flare : June 2015

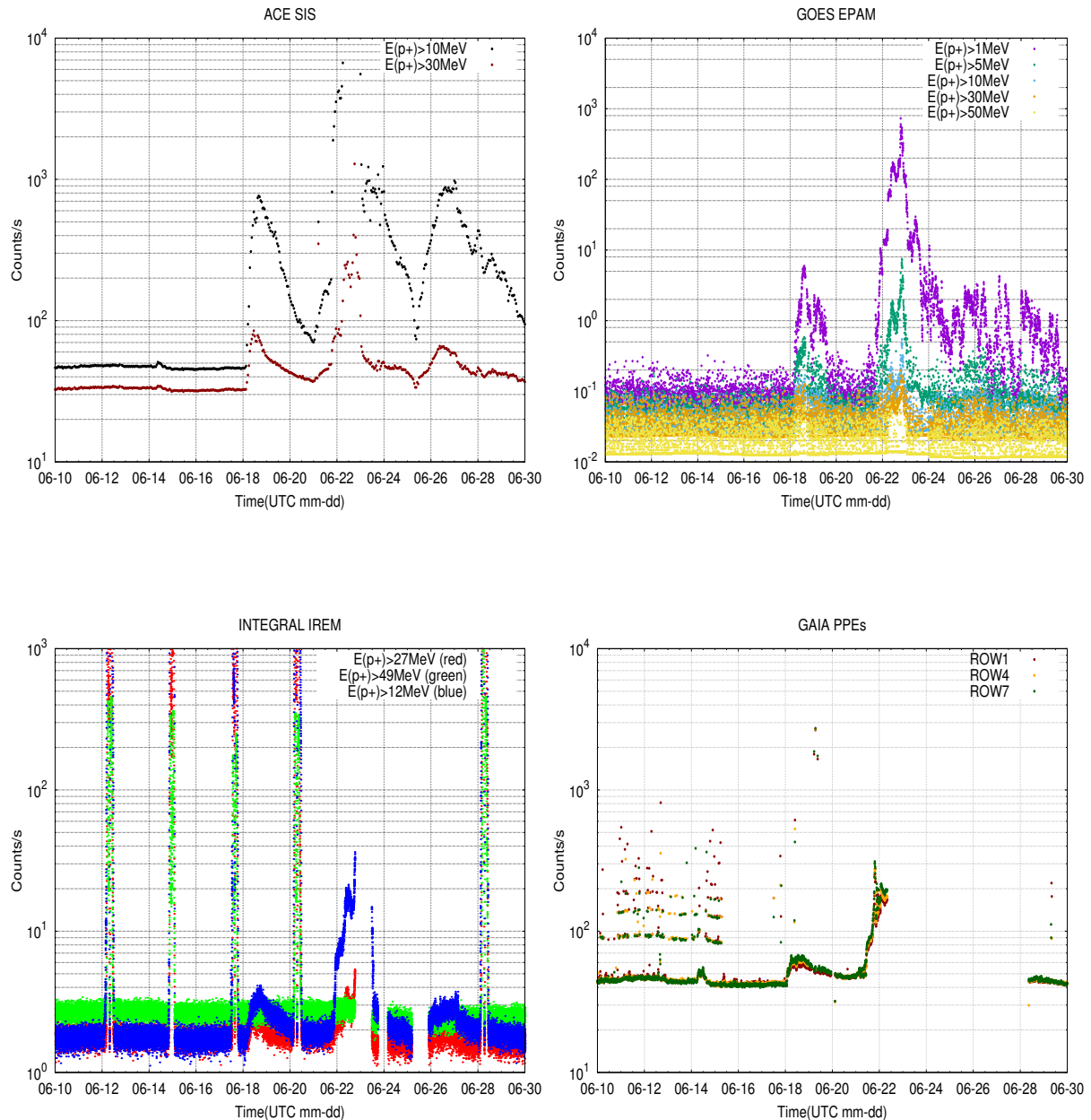


Figure 18: Particle Count Rates from ACE SIS (top left), GOES EPAM (top right), INTEGRAL SREM (bottom left : vertical features are radiation belt crossings) and GAIA PPEs (bottom right) for June 2015 Solar Event.

We can distinguish for all events, a first phase where the shock wave (caused by and) preceding the CME triggers a moderate increase in particle rates. Then this is followed by a decay with certain time constant that can vary from hours to days depending in the strength of the event, and finally the CME hitting the spacecraft resulting in a sharp increase in the measured cosmics rate.

The 'radiation profiles' are comparable amongst different instruments in all major events specially in the 10-30 MeV proton energy band. The incident distribution of Solar Proton radiation will clearly contain more components but the similarity between the Gaia PPE profiles and the 10-30 MeV bands of other instruments seems to indicate that lower energy particles simply get stopped by the spacecraft's shielding while higher energy protons would reach the FPA but leave fast enough so as to deplete little or not enough charge to trigger an actual object detection at CCD level.

4.2 Solar Particle Event Energy Distribution at L2 ?

Following the previous section we should now compute the Solar proton budget measured by Gaia during Solar particle events and compare it to those measured by the other spacecrafts for the same periods in the range $10 < E(p+) < 30$ MeV.

The total Solar proton budget as measured by Gaia during these Solar Events can be computed by subtracting the PPEs background , the galactic cosmic rays, to the total count rate measured on each SM CCD and FOV , and then adding each of those contributions (for the 7 SM CCDs and 2 FOVs) The PPE background at time t is obtained from Table 2. This can be expressed as follows:

$$N_{p+}(t)[10 - 30\text{MeV}][\text{FOV}] \simeq \sum_{n=1}^7 (\text{PPE}_n[\text{FOV}](t) - \text{Background}_n[\text{FOV}](t)) \quad (5)$$

Results of this computation have been plotted together with the other's spacecrafts solar proton counts for 3 of the 4 selected solar events. Note that June 2015 has a significant (days) ASD4 data gap which does not allow to perform such calculation and hence is not included in the comparisons:

Energy Distribution Comparisons:

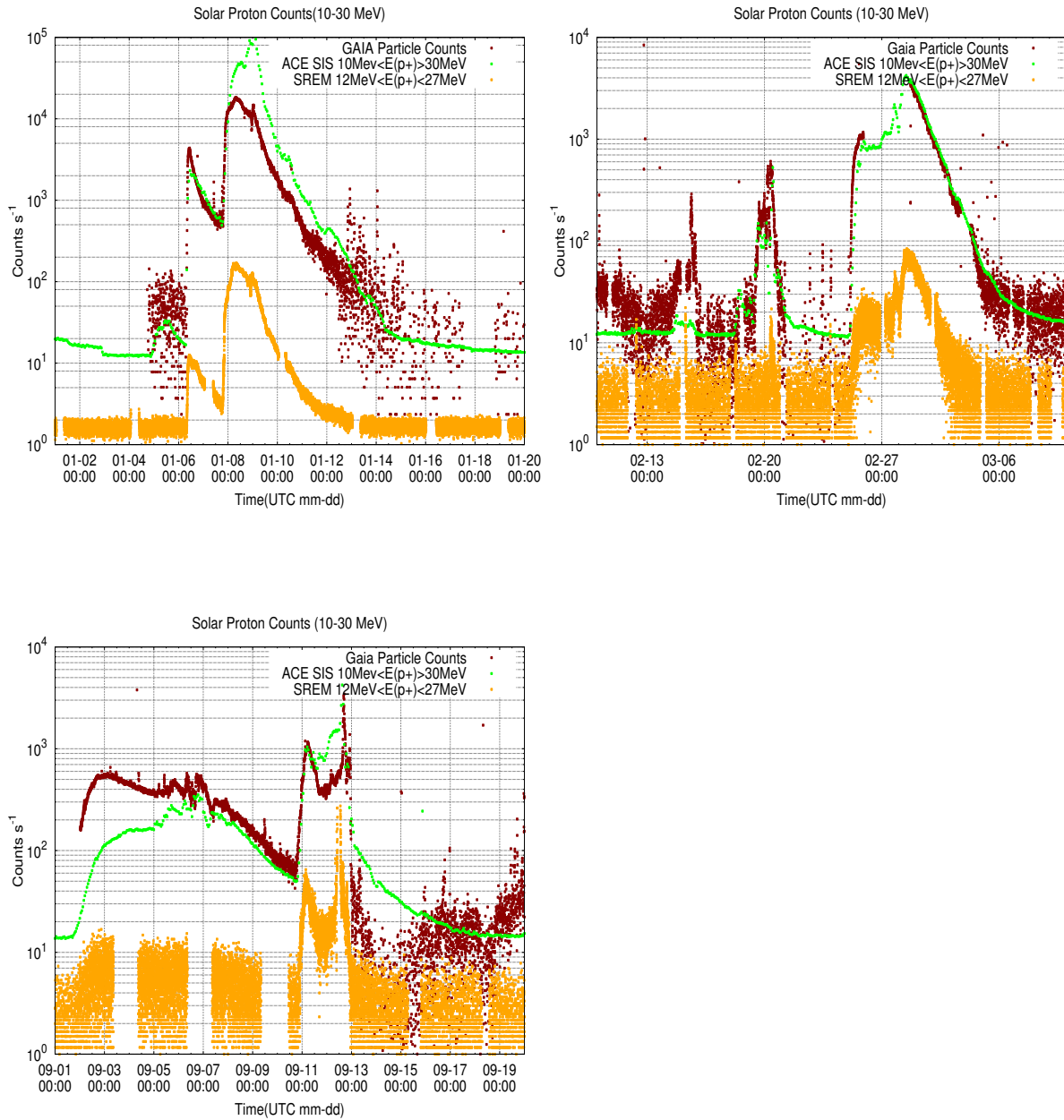


Figure 19: Energy Distribution comparisons for 3 out of the 4 events studied. Gaia PPEs (red), ACE SIS (green) and SREM (orange), GOES EPAM falls outside the scale.

The better correlation seems to be systematically with the ACE SIS instrument at L1. Some events show a very good agreement between Gaia PPEs and ACE SIS counts (Feb 27th 2014 difference of less than 10% in almost the full extent of the event), in others though there is a large deviation of up to a factor of 2 or even more, especially during the peak intensity of the event. Count rates from IREM and EPAM

data show a systematic a deficit in proton count as compared to the Gaia PPE counters.

Both GOES and INTEGRAL , are Earth orbiting satellites, the first on geostationary orbit (36000 Km) and a highly elliptical orbit with a perigee of approximately 175000 Km in the case of INTEGRAL, therefore more influenced by Earth's magnetic field than ACE spacecraft in L1.

5 Conclusions

We have studied the long term behavior of the Gaia Prompt Particle Event counters available in the ASD4 data for a period of 1.5 years since Launch. The PPEs pedestal has experienced a progressive increase since early 2014 (Fig. 3) which anti-correlates with the solar activity evolution in the same period indicating that it corresponds to Galactic Cosmic Rays. These get 'blocked' by a stronger Sun magnetic field during solar maxima but penetrate further into the inner Solar System as solar activity decreases, the case currently, resulting in increased PPEs pedestal level.

We provide first order approximations of predicted particle count rates at future times in the mission in Table. 2) and compared them with actual measured rates (Fig 5).

We showed how the periodic features also detectable in the long term analysis of the PPEs can be explained by false detections induced by increased stray-light levels coming either the Sun (Fig. 8) or Milky-Way (Fig. 7).

We finally compared the radiation environment measured by Gaia to that measured by instruments on-board other spacecrafts for the same period and found relatively good agreement with the 10-30 MeV proton fluxes as measured by ACE SIS instrument at L1. (Fig. 19).

Although the similarity is very good in some cases, there is not enough evidence or not so compelling to assert that Gaia PPE counters are measuring protons *only* in the range 10-30 MeV during solar events. A further analysis of shielding would be required to constrain at least the lower energy bound of protons actually able to reach the FPA through the shielding.

Future Work

We plan to make a quantitative assessment of the stopping power of the DSA and Thermal Tent materials to determine minimum energies of trespassing protons actually reaching the FPA. We also plan to make estimates of energy deposited in the Gaia CCDs during these solar events by some alternative methods to gain insight in the energy 'spectrum' of the cosmic rays at L2. Further strong solar events will be analyzed in the context of radiation damage monitoring in the Gaia CCDs.

6 References

[**GAIA.ASF.UM.PLM.00022**], Airbus DS, 2015, *Video Processing Algorithm user manual*,

GAIA.ASF.UM.PLM.00022,

URL <http://www.rssd.esa.int/cs/livelink/open/3014813>

[**BAS-003**], Bastian, U., 2007, *Reference systems, conventions and notations for Gaia*,

GAIA-CA-SP-ARI-BAS-003,

URL <http://www.rssd.esa.int/cs/livelink/open/358698>

[**AB-049**], Brown, A., Jordan, S., 2014, *Stray light modulations caused by diffracted sun light*,

GAIA-CA-TN-LEI-AB-049,

URL <http://www.rssd.esa.int/cs/livelink/open/3256532>

Davis, A., Mewaldt, R., Cohen, C., et al., 2001, In: International Cosmic Ray Conference, vol. 10, 3971

Heber, B., Kopp, A., Gieseler, J., et al., 2009, *The Astrophysical Journal*, 699, 1956

Horeau, B., Boulade, O., Claret, A., et al., 2011, In: Radiation and Its Effects on Components and Systems (RADECS), 2011 12th European Conference on, 541–548, IEEE

ONeill, P., Golge, S., Slaba, T., 2015

Paul Buhler, A., W.Hadjas, 1998, *Technical note on WP 81*, Tech. rep., PSI

Rodriguez, J., Onsager, T., Mazur, J., 2010, *Geophysical Research Letters*, 37

[**FVL-144**], van Leeuwen, F., 2015, *Cosmic-Ray hit detections around the 10 September 2014 solar flare event*,

GAIA-C5-TN-IOA-FVL-144,

URL <http://www.rssd.esa.int/cs/livelink/open/3362011>

Zwickl, R., Doggett, K., Sahm, S., et al., 1998, *Space Science Reviews*, 86, 633